Nano Today 63 (2025) 102748

Contents lists available at ScienceDirect

Nano Today

journal homepage: www.elsevier.com/locate/nanotoday

Tumor cell-derived engineered exosome enhances effective immunotherapy for orthotopic glioblastoma and its recurrences

Shanshan Li [a], Dongya Zhang [a], Yibin Wang [a], Muhammad Ismail [a], Wenya He [a], Meng Zheng [a], Bingyang Shi [a,b,*], Yan Zou [a,c,*]

[a] Henan-Macquarie Uni Joint Centre for Biomedical Innovation, Henan International Joint Laboratory of Nanobiomedicine, Henan Key Laboratory of Brain Targeted Bio-Nanomedicine, School of Life Sciences, Henan University, Kaifeng, Henan 475004, China
[b] School of Biomedical Engineering, University of Technology Sydney, Sydney, NSW 2007, Australia
[c] Macquarie Medical School, Faculty of Medicine, Health and Human Sciences, Macquarie University, Sydney, NSW 2109, Australia

ARTICLE INFO

Keywords:
Glioblastoma
Exosomes
Recurrences
Immune responses
Immunotherapy

ABSTRACT

Glioblastoma multiforme (GBM) is considered as one of the most lethal malignancies in the central neuron system (CNS). Despite significant advances in immunotherapy approaches for multiple tumors, the highly immunosuppressive tumor microenvironment (TME) of GBM presents critical challenges. Inspired by tumor-derived exosomes, which carry a range of tumor-associated antigens and possess improved blood-brain barrier (BBB) transcytosis, we have developed CpG adjuvant-functionalized GBM tumor-derived exosomes (Exo-CpG) to inhibit GBM proliferation and elicit long-lasting protective immunity via potent stimulation of the body's innate immunity. Our exosomal nanoplatform efficiently activates the antigen-presenting dendritic cells (DCs) in lymph nodes, promoting their maturation, and generating a strong T cell response. In combination with the anti-programmed cell death ligand-1 antibody (aPD-L1), these exosomes effectively restrain the growth of GBM in orthotopic primary GL261 and phosphatase and tensin homologue (PTEN)-deficient immunosuppressive CT2A models in immune-competent mice, significantly prolonging survival by effectively suppressing GBM recurrence. This fully natural exosomal nanoplatform offers a promising strategy for targeting the immunosuppressive TME of orthotopic primary GBM and its recurrences.

Introduction

Glioblastoma multiforme (GBM) is the most common primary malignant tumor in the central nervous system (CNS) [1,2] and is characterized by high infiltration and poor prognosis, resulting in a high recurrence rate [3–5]. The standard of care for newly diagnosed GBM patients is surgical resection followed by chemotherapy and radiotherapy. However, the median survival has not been markedly improved and is still less than 15 months [6,7]. Although recent developments in immunotherapy approaches (immune checkpoint inhibitors, chimeric antigen receptor T (CAR-T)) have shown positive treatment outcomes towards melanoma and breast cancers, these approaches remain disappointing for GBM. For example, the Phase III clinical trial CheckMate 143, which tested anti-PD-1 therapy in GBM patients, yielded comparable median overall survival (mOS) and worse median progression-free survival (mPFS) compared to placebo [8]. These failures are mainly attributed to the heterogeneity of GBM, its immunosuppressive TME with low tumor immunogenicity and poor lymphocyte infiltration, together with the existence of blood-brain barrier (BBB) [9], all contributing to suboptimal immune responses in most patients. Therefore, an effective strategy to improve the immunosuppressive tumor microenvironment (TME) is urgently needed.

Exosomes, which are subpopulation extracellular vesicles (EVs) ranging from 30 to 200 nm, are secreted by various cells and can be absorbed by receptor cells [10,11]. Due to their excellent biocompatibility and intercellular permeability, exosomes have been developed as multifunctional natural carriers for cancer diagnosis and treatment [12–14]. Importantly, tumor-derived exosomes inherit the membrane protein profile of donor cells [15], enabling them to actively target homologous tumor tissues/cells, and carry multiple tumor antigen information [16–18]. For instance, a clinical trial based on tumor-derived exosomes (NCT01344109) aims to use these vesicles as diagnostic and

* Corresponding authors at: Henan-Macquarie Uni Joint Centre for Biomedical Innovation, Henan International Joint Laboratory of Nanobiomedicine, Henan Key Laboratory of Brain Targeted Bio-Nanomedicine, School of Life Sciences, Henan University, Kaifeng, Henan 475004, China.
E-mail addresses: bs@henu.edu.cn (B. Shi), yzou@henu.edu.cn (Y. Zou).

https://doi.org/10.1016/j.nantod.2025.102748
Received 12 November 2024; Received in revised form 25 March 2025; Accepted 28 March 2025
Available online 8 April 2025

prognostic markers in breast cancer patients receiving neoadjuvant chemotherapy [19]. Remarkably, tumor exosomes are typically phagocytosed by dendritic cells (DCs), utilizing these cells as intermediaries to activate tumor antigen-specific T cells, thereby generating antitumor immune responses and long-lasting memory immune T cells [20,21]. Previous work, including our own, has reported that exosomes derived from various cells, including mesenchymal stem cells (MSCs) [22], macrophages [23,24], dendritic cells [25] and tumor cells [26], exhibit high BBB permeability [27]. Specifically, tumor-derived exosomes demonstrate superiority in treating GBM, benefiting from their immune activation and excellent BBB crossing capability. However, they are rarely reported in GBM treatment without carrying extra drugs or antigens.

In this work, we propose for the first time a versatile platform based on natural GBM-derived exosomes for immunotherapy against primary GBM and its recurrences. Consequently, the Exo loaded with CpG can be taken up by dendritic cells, where CpG subsequently exerts its effects within those cells by specifically stimulating Toll-like receptor 9 (TLR9) to enhance the immune response and induce both cellular and humoral immunity [28–30]. Additionally, the multiple natural tumor-associated antigens on the exosome surface trigger a strong immune response, further amplified by the CpG adjuvant stimulation (Fig. 1). Overall, the resulting Exo-CpG effectively permeates the BBB, and potentially accumulate in the brain tumor niches. When combined with PD-L1 immune checkpoint inhibitor antibody, Exo-CpG demonstrate efficient antitumor efficacy, and elicite robust immune responses in both GL261 and PTEN-deficient immunosuppressive CT2A GBM mouse models. Furthermore, these exosomes significantly prevent the risk of post-operative recurrence of GBM and prolong survival. Altogether, this fully natural exosomal nanoplatform provides a potent and straightforward strategy for treating immunosuppressive GBM and its recurrences.

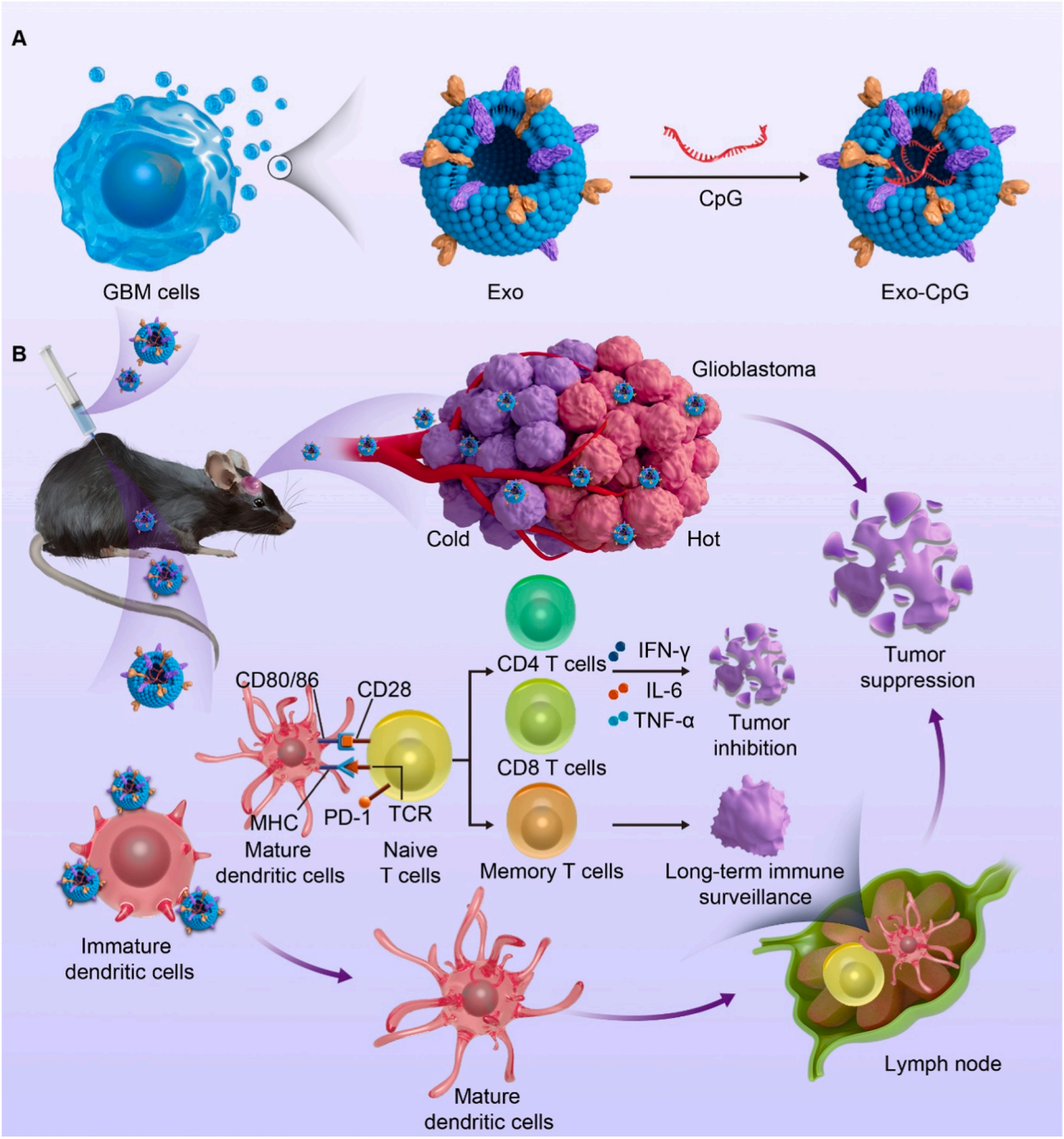

Fig. 1. Natural GBM-derived exosomes are readily decorated with CpG, effectively activate the anti-tumor immune responses via enhancing antigen presentation, promoting the generation of $CD4^+$ and $CD8^+$ T cells, and facilitating the secretion of cytokines. All these lead to tumor suppression and the establishment of long-term memory immune surveillance.

Results and discussion

CpG-loaded tumor cell-derived exosomes (Exo-CpG) leverage efficient cellular uptake and in vitro permeability

Exosomes (Exo) were readily extracted from GBM tumor cells via centrifugation, as described in previous reports [31–33]. Transmission electron microscopy (TEM) images confirmed that the exosomes possess a characteristic lipid bilayer structure (Fig. 2A). Dynamic light scattering (DLS) measurement indicated that the Exo have an average size of approximately 65 nm (Fig. 2B). Western blot results and sodium dodecyl sulfate-polyacrylamide gel electrophoresis (SDS-PAGE) demonstrated that the protein profile of GL261-derived Exo closely resembles the parental GL261 whole-cell protein, indicating that the proteins were well retained during Exo production (Fig. 2C, Figure S1). These findings align with previous reports, suggesting that tumor cell-derived Exo successfully retain tumor antigens [34–36]. Subsequently, we employed the electroporation method to encapsulate the adjuvant CpG within the interior of Exo, effectively preventing the degradation of CpG and ultimately synthesizing a stable Exo-CpG complex. The CpG encapsulation efficiency was quantified as 60 % via Nanodrop spectrophotometry. The hydrodynamic diameter of Exo-CpG reached 70 nm, slightly higher than naked exosomes (Fig. 2B). Agarose gel electrophoresis further confirmed the successful encapsulation of CpG (Figure S2). The adjuvant CpG encapsulated into exosomes enables the augmented stimulation of immune responses.

Exo-CpG presented efficient cellular uptake in dendritic cells (DCs) through endocytosis (Figure S3), which is crucial for triggering DCs' maturation. Additionally, we successfully constructed a 3D spheroid model using DC2.4 cells (Fig. 2D). In this model, Cy5-loaded Exo-CpG demonstrated significant penetration and deeply infiltrated the spheroid, while free CpG exhibited limited permeability (Fig. 2E). Quantitative analysis revealed a statistically significant difference between the fluorescence intensity of delivered Cy5 by Exo-CpG and free CpG (Fig. 2F). Importantly, Exo-CpG also showed time-dependent active uptake by GL261 GBM tumor cells, with internalization efficiency increasing gradually over extended incubation periods (Fig. 2G). Interestingly, the Exo-CpG effectively promoted the repolarization of M2-type tumor-associated macrophages (TAMs) towards the M1 phenotype (Figure S4), which is capable of secreting a variety of pro-inflammatory cytokines and in turn augmenting the infiltration of T cells and dendritic cells [37,38].

Exo-CpG exhibit effective BBB penetration and tumor accumulation

Exosomes have been shown to penetrate the BBB, effectively targeting and accumulating at the relevant tumor sites [18,39,40]. To further confirm this, we evaluated the BBB permeability of Cy5-CpG-encapsulated Exo-CpG using an *in vitro* transwell model (Fig. 3A). The results showed that the Exo-CpG demonstrated a significantly higher transport ratio versus free CpG at all time intervals, supporting its potential to traverse the BBB (Fig. 3B). Furthermore, Exo-CpG

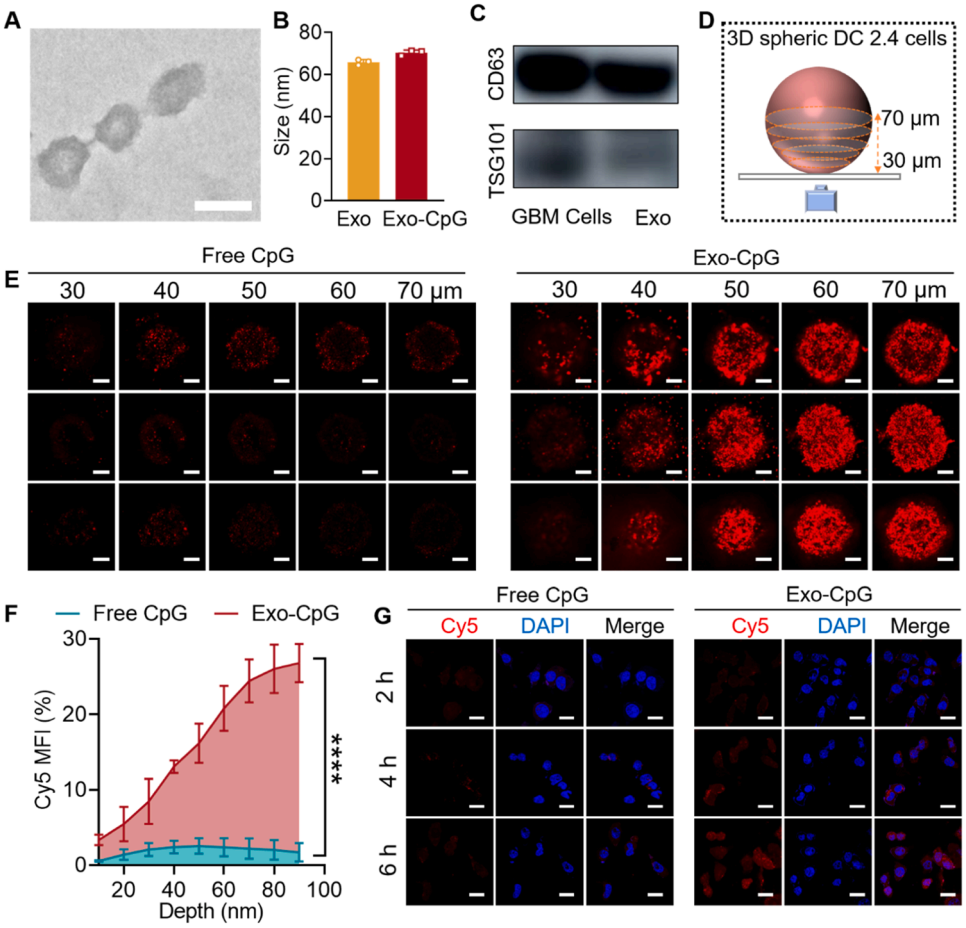

Fig. 2. Exo-CpG demonstrates effective cellular uptake and *in vitro* permeability. (A) Morphology of Exo determined by TEM (scale bar: 100 nm). (B) Hydrodynamic size distributions of Exo and Exo-CpG. (C) Protein markers in the GBM tumor cells derived Exo detected by western blotting. (D) Schematic illustration showing the 3D spherical model of DC2.4 cells. (E) Imaging and (F) quantification of Cy5-loaded Exo-CpG penetration in the 3D spheroid model following 6 h incubation (Cy5-loaded CpG concentration: 0.025 mg mL^{-1}, scale bar: 100 μm). The data are presented as mean ± SD (n = 3). (G) CLSM image for the GL261 cells after 2, 4 and 6 h incubation with Exo-CpG (Exo concentration: 0.12 mg mL^{-1}, Cy5-loaded CpG concentration: 0.025 mg mL^{-1}). Scale bar: 20 μm.

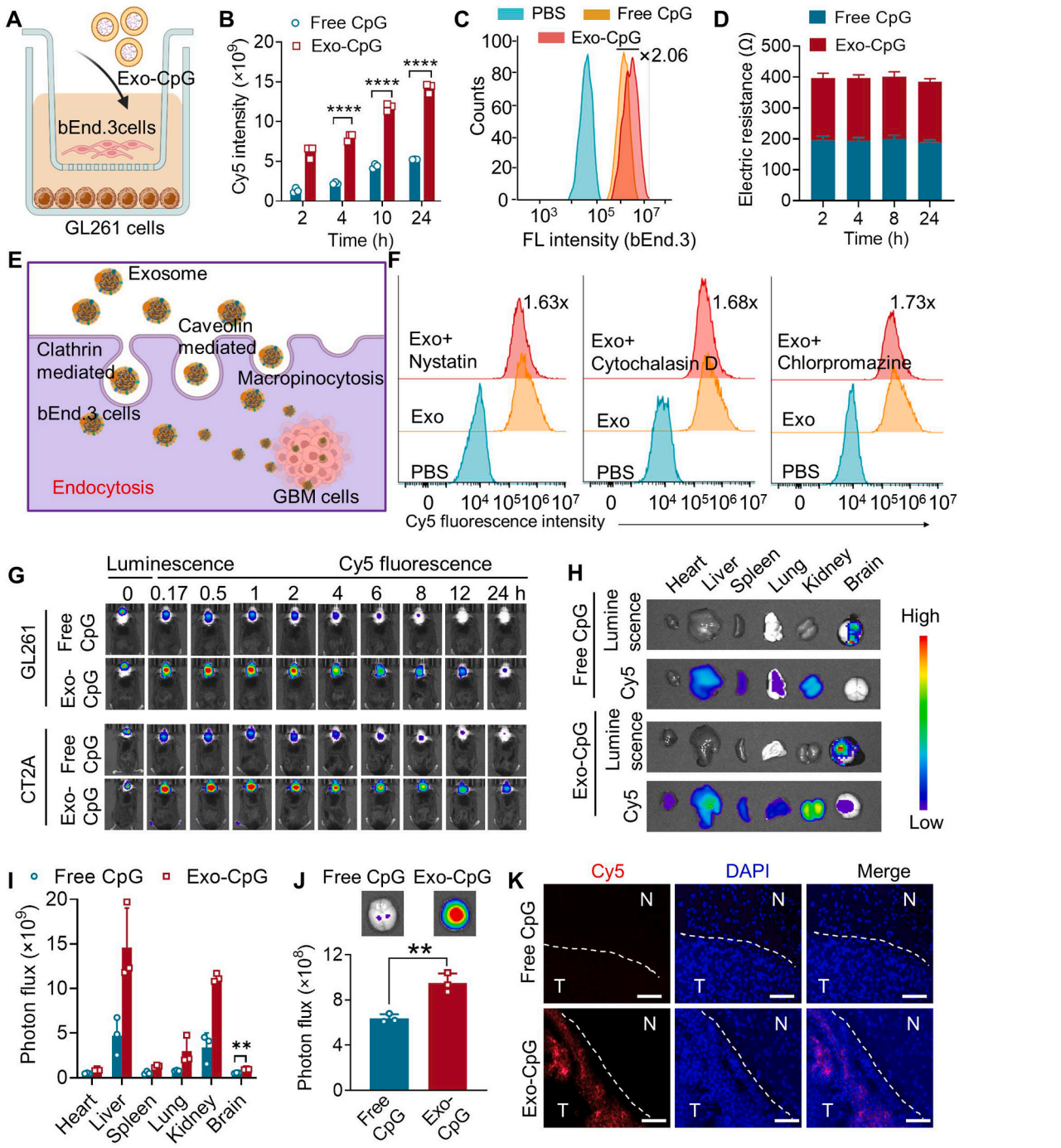

Fig. 3. Exo-CpG show enhanced BBB penetration and brain tumor accumulation. (A) Schematic diagram showing the construction of *in vitro* BBB transwell model. (B) The fluorescence intensity of Cy5-loaded Exo-CpG transferred to the lower chamber at different time intervals (2, 4, 10 and 24 h, n = 3). (C) Cellular uptake of Exo-CpG by bEnd.3 endothelial cells in the upper chamber of transwell model. (D) Transepithelial electrical resistance (TEER) values of BBB monolayer monitored during the course of experiment. (E) Exo-CpG exosomes pass through the BBB via multiple-pathway transcytosis. (F) Cellular uptake of Cy5-loaded Exo in the bEnd.3 endothelial cells with or without pretreatment with endocytic inhibitors (Nystatin, Chlorpromazine and Cytochalasin D). (G) *In vivo* fluorescence imaging of mice bearing GL261-luc and CT2A-luc tumors administered with Cy5-loaded Exo-CpG at different time points. (H) *Ex vivo* fluorescence imaging and (I) the quantification of the *ex vivo* fluorescence in the major organs (heart, lung, spleen, liver, kidney and brain) at 0.5 h post-injection with Cy5-labeled Exo-CpG. (J) Magnified *ex vivo* Cy5-fluorescence imaging and their quantification of dissected brains following treatment with Exo-CpG or naked CpG. (K) Tumor tissue penetration behaviour of Cy5-labeled Exo-CpG observed by CLSM (Scale bar: 200 μm).

demonstrated superior cellular uptake compared to free CpG, with a 2.06-fold increase in bEnd.3 cells (upper chamber) and a 1.43-fold increase in GL261 GBM cells (lower chamber), respectively (Fig. 3C, Figure S5). Interestingly, the trans-endothelial electrical resistance (TEER) value remained relatively stable after treatment with Exo-CpG, indicating that the integrity of transwell model was maintained intact (Fig. 3D). These results suggest that the exosomes may pass through the BBB primarily via transcytosis associated transcellular mechanisms, consistent with previous reports [23,41,42]. To further reveal the mechanism underlying BBB transcytosis, we evaluated the cellular uptake of exosomes in endothelial cells using different endocytosis inhibitors. As shown in Fig. 3E, the cellular uptake of exosomes was

remarkably inhibited after pretreated with all these inhibitors, showing reductions of 1.63-, 1.68-, and 1.73-fold for caveolin (Nystatin), macropinocytosis (Cytochalasin D), and clathrin (Chlorpromazine), respectively (Fig. 3F, Figure S6). Additionally, the cellular uptake of Exo-CpG was markedly reduced in DC2.4 cells pretreated with inhibitors, indicating these exosomes enter cells via multiple endocytosis pathways (Figure S7), including clathrin-mediated endocytosis, caveolin-mediated endocytosis as well as macropinocytosis, which are also verified by others that the exosomes prefer to be internalized by cells rather than membrane fusion [43,44].

To further evaluate the BBB permeability and tumor-targeting ability *in vivo*, Cy5-labeled Exo-CpG was injected into mice bearing orthotopic GL261-luc GBM. Notably, Exo-CpG showed a stronger fluorescence signal in the brain site that sustained up to 24 h, whereas free CpG was hardly detectable at the 12 h time point (Fig. 3G). The *ex vivo* imaging was performed at 30 min as the brain accumulation of exosomes peaked at this point among the long-term monitoring intervals (Figure S8). Similar results were observed in the CT2A-luc mouse model, in which Exo-CpG demonstrated enhanced brain tumor accumulation.

Subsequently, *ex vivo* imaging of major organs (heart, liver, kidney, lung, spleen and brain) revealed obvious Cy5 signals visualized in the brains of mice treated with Exo-CpG. In sharp contrast, there was only

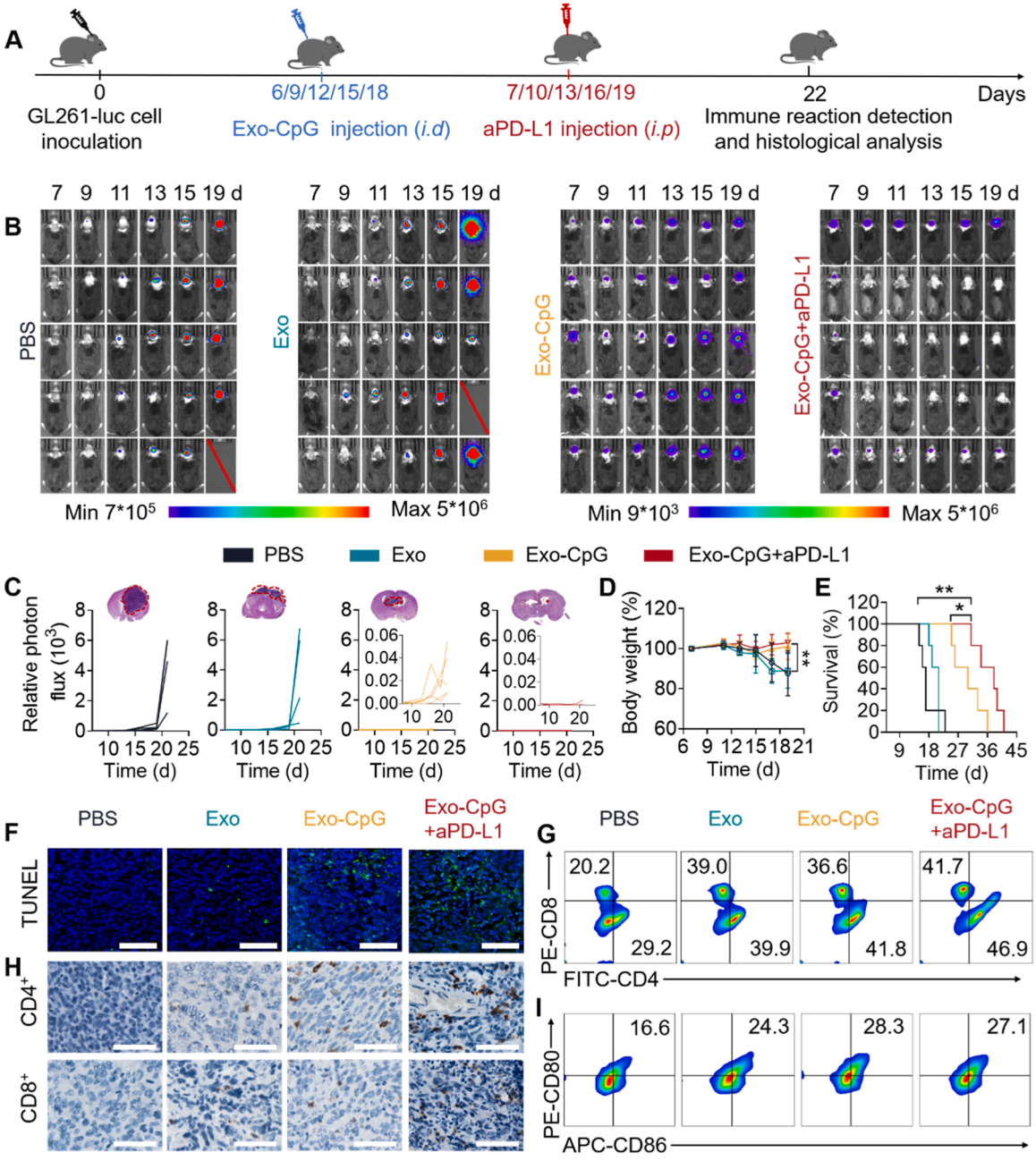

Fig. 4. Therapeutic effects of Exo-CpG in orthotopic GL261-luc tumor-bearing mice. (A) Treatment timeline for orthotopic GL261-luc tumor-bearing mice receiving Exo-CpG via the intradermal injection (*i.d.*) every three days for 5 cycles. The aPD-L1 antibody was administered intraperitoneally (*i.p.*), following the Exo-CpG (Exo: 7.5 mg kg^{-1}, CpG: 0.8 mg kg^{-1}, aPD-L1: 1.75 mg kg^{-1}). (B) Bioluminescence images and (C) relative bioluminescence intensity measured using the Lumina IVIS III system; the inset images show the H&E-stained brain slices. (D) Body weight and (E) survival curves of the treated mice. (F) TUNEL-staining of GL261-luc tumor sections post-treatment (scale bar: 50 μm). (G) Representative flow cytometry dot plots show $CD4^+$ and $CD8^+$ T cells in the blood. (H) IHC assessment of $CD4^+$ and $CD8^+$ T cell subsets of GL261-luc tumor sections following treatments (scale bar: 50 μm). (I) Representative flow cytometry dot plots of CD80 and CD86 cells in lymph nodes.

faint fluorescence in the brains of mice treated with free CpG (Figs. 3H, 3I). Quantitative fluorescence measurements further verified that Exo-CpG had a remarkably stronger brain accumulation as compared to free CpG (Fig. 3J). Importantly, Exo-CpG displayed deep penetration at the tumor site, resulting mainly from the excellent BBB permeability (Fig. 3K). Collectively, these results evidenced that the developed Exo could efficiently pass through the BBB and target GBM tumor lesions to potentially alleviate the immunosuppression.

Immunotherapy effects in orthotopic GL261-luc GBM mouse model

The efficient BBB permeability of Exo-CpG prompted us to investigate their antitumor effects in orthotopic GBM mouse models. GL261-luc cells, which stably express luciferase, were inoculated into C57BL/6 immune-competent mice (Fig. 4A). To assess treatment outcomes, the commercial immune checkpoint inhibitor anti-programmed cell death ligand-1 antibody (aPD-L1) was administrated to combine with Exo-CpG. The aPD-L1 was administered one day after exosomes as the immune responses could be quickly activated, which was similar to other report [45]. Bioluminescence imaging and quantification of relative bioluminescence intensity showed that the Exo alone or PBS exhibited negligible tumor inhibition. In contrast, Exo-CpG partially inhibited the tumor growth, resulting in a slower progression during the treatment period. However, when combined with aPD-L1, Exo-CpG completely suppressed the tumor growth, as indicated by reduced bioluminescence intensity within a week (Fig. 4B). Importantly, three of the five treated mice lost the tumor signal after receiving Exo-CpG plus aPD-L1, exhibiting limited tumor growth (Figs. 4B, 4C). The combinatorial treatment of Exo-CpG+aPD-L1 resulted in a significant tumor shrinkage as detected by H&E staining of whole brain slices collected on day 22 (Fig. 4C). Additionally, the body weight of mice treated with Exo alone or PBS reduced rapidly due to the fast tumor propagation that induced dysfunction in normal brain tissues (Fig. 4D). In contrast, negligible weight changes were observed in mice treated with Exo-CpG with or without aPD-L1, highlighting their effective tumor suppression. More importantly, Exo-CpG+aPD-L1 markedly extended the mice's survival with a prolonged median survival time (MST) of 38 days, which was significantly longer than that of Exo-CpG (30 days), Exo alone (21 days), or PBS (17 days) (Fig. 4E). TUNEL staining further corroborated the presence of abundant apoptotic tumor cells in the Exo-CpG+aPD-L1 group (Fig. 4F). In parallel, H&E staining of major organs, including the heart, liver, spleen, lung and kidney revealed no significant side effects (Figure S9), supporting the excellent biocompatibility of the developed exosomes.

To further study the immune responses, we assessed T cell levels in the blood as well as the activation capacity of DCs in the mesenteric lymph nodes. As expected, mice treated with Exo-CpG+aPD-L1 had the higher ratios of cytotoxic T cells ($CD8^+$) and helper T cells ($CD4^+$) in the blood (88.6 % of total T cells) than that of PBS (49.2 %) (Fig. 4G, Figure S10). Immunohistochemistry (IHC) analysis further validated the increased number of $CD4^+$ and $CD8^+$ T lymphocytes in brain tumor tissues, following treatment with Exo-CpG+aPD-L1 (Fig. 4H, Figure S11). Interestingly, both Exo alone and Exo-CpG in the presence of aPD-L1 induced similar levels of cytotoxic T cells, primarily due to the immune activation triggered by the exosomes.

It is well-known that DCs play an important role in enhancing the immune response in tumor-draining lymph nodes (TDLN) and facilitating tumor infiltration [46–48]. We therefore tested the expression of CD86 and CD80, markers of mature DCs in mesenteric lymph nodes. Exo-CpG+aPD-L1 resulted in significantly higher CD86 and CD80 levels versus PBS or Exo and comparable to Exo-CpG alone, indicating that tumor antigens and CpG delivery promoted the DCs' maturation *in vivo* (Fig. 4I, Figure S12), which is consistent with other reports [49,50]. Taken together, CpG functionalized tumor exosomes plus aPD-L1 efficiently stimulate strong DCs maturation, induce antigen cross-presentation, and achieve potent GBM immunotherapy, resulting in improved mice's survivability with negligible side effects.

Immunotherapy effects in immunosuppressive orthotopic CT2A-luc GBM mouse model

CT2A-luc GBM cells, characterized by phosphatase and tensin homolog (PTEN) deficiency, exhibit an immunosuppressive tumor microenvironment that is resistant to immunotherapy [51,52]. Thus, a CT2A-luc GBM animal model was constructed to assess whether CpG-modified exosomes could activate the immune system in immunosuppressive mice.

The administration of Exo-CpG in the CT2A-luc GBM model was analogous to that of the GL261-luc model (Fig. 5A). As illustrated in Figs. 5B, 5C, mice treated with Exo-CpG plus aPD-L1 had the slowest tumor growth among all groups. While Exo-CpG could partially restrain tumor growth, its efficacy was less potent than the combination with aPD-L1. Robust tumor suppression was evidenced by H&E staining of brain slices, revealing the smallest tumor volume in the Exo-CpG+aPD-L1 treatment group. Furthermore, none of the exosomes altered the body weight of the mice during the treatment period (Fig. 5D). Intriguingly, the mice's survival was significantly extended after the injection of Exo-CpG combined with aPD-L1, resulting in improved median survival time of 49 days, surpassing that of Exo-CpG (41 d), Exo alone (30 d) and PBS (30 d) (Fig. 5E). Analogous to the GL261-luc mouse model, Exo-CpG plus aPD-L1 induced multiple apoptotic signals in tumor cells by day 22 (Figure S13). No significant organ damage or inflammatory injury was observed in the major organs (Figure S14), suggesting that Exo-CpG+aPD-L1 could safely achieve robust antitumor effects in the immunosuppressive CT2A-luc tumor.

Next, the immunological stimulation of the Exo-CpG in CT2A-luc mouse models was assessed by analyzing immune cells from blood, spleen, and lymph nodes on day 22, via flow cytometry. Mice treated with Exo-CpG+aPD-L1 displayed a 1.96-fold increase in $CD4^+$ and $CD8^+$ T cells in the blood of mice compared to the PBS group (Fig. 5F, Figure S15A). Additionally, Exo-CpG+aPD-L1 induced a 1.70-fold increase in $CD44^{Hi}$ and $CD62^{Low}$ populations (Fig. 5G, Figure S15B) and a 1.93-fold upsurge in CD80 and CD86 cells, further indicating that the exosomes triggered strong immune memory and effective DC maturation effects (Fig. 5H, Figure S15C). The enhancement in cytotoxic T cells was further confirmed by the IHC staining of the tumor, highlighting that Exo-CpG+aPD-L1 had a higher percentage of T cells at the tumor site (Fig. 5I, Figure S16). Intriguingly, this treatment combination also caused abundant cytotoxic T cells in the spleen (Figure S17). Expectedly, the spleens of mice treated with Exo-CpG+aPD-L1 were larger and heavier versus controls, while overall body weight remained stable (Fig. 5J-L). This enlargement of the spleen, the body's largest immune organ, reflects its crucial role in generating systemic immunity. Collectively, the excellent anti-GBM effects in the immunosuppressive CT2A-luc mouse model could be attributed to the strong DCs maturation and enhanced antigen cross-presentation, effectively transforming the "cold" into "hot" GBM immune microenvironment, making it favorable to immune attack.

Immunotherapy effects in immunosuppressive orthotopic CT2A-luc GBM tumor resection model

GBM almost inevitably recurs after surgery, and becomes more aggressive upon recurrence [53]. A clinically relevant recurring model was successfully constructed, and the tumor in the model was subsequently surgically removed, as confirmed by IVIS imaging (Figure S18). Following surgery, the Exo-CpG was administered intradermally (*i.d.*) into the mice bearing recurrent GBM for a total of five doses, together with aPD-L1 via intraperitoneal (*i.p.*) injection (Fig. 6A). Notably, tumor growth was significantly delayed in mice treated with Exo-CpG compared to those receiving PBS or Exo alone. Most importantly, the combination of Exo-CpG with aPD-L1, potentially retarded tumor

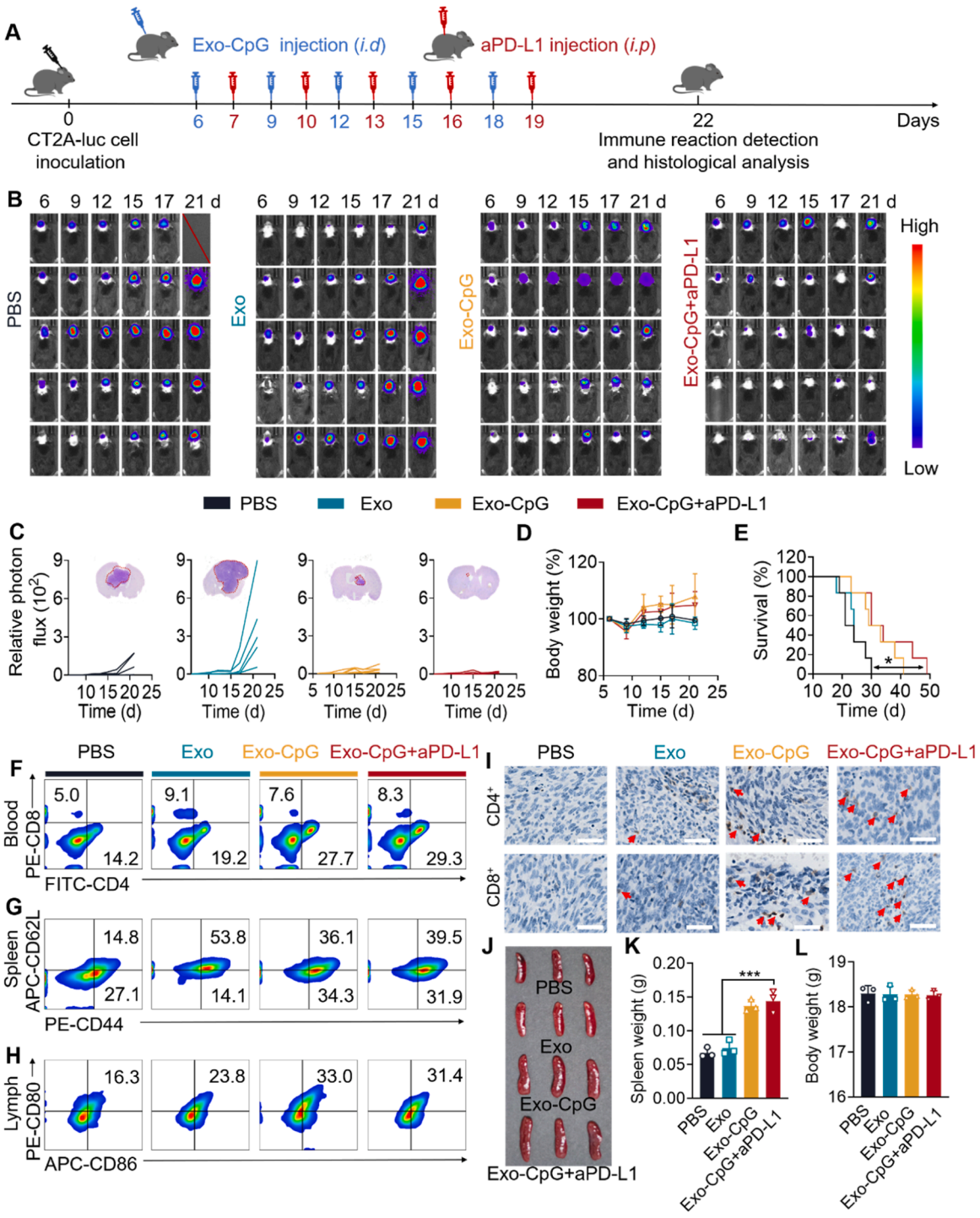

Fig. 5. Therapeutic effects of Exo-CpG in immunosuppressive orthotopic CT2A-luc tumor-bearing mice. (A) Treatment scheme for orthotopic CT2A-luc tumor-bearing mice treated with Exo-CpG, Exo-CpG plus aPD-L1, Exo alone and PBS via the intradermal injection (*i.d.*) every three days for five doses. Exo-CpG (Exo: 7.5 mg kg^{-1}, CpG: 0.8 mg kg^{-1}, aPD-L1: 1.75 mg kg^{-1}) was administered prior to the aPD-L1 antibody via intraperitoneal (*i.p.*) injection. (B) Bioluminescence images and (C) quantification of relative bioluminescence intensity obtained via Lumina IVIS III system; the inset images show tumor burden stained with H&E. (D) Body weight and (E) survival curves of treated mice. (F) Representative flow dot plots of $CD4^+$ and $CD8^+$ T cells in the blood. (G) Flow dot plots of $CD62^{Low}$ and $CD44^{Hi}$ effector memory T cells in the spleen and (H) flow dot plots of CD80 and CD86 cells in lymph nodes (on day 22). (I) IHC staining of $CD4^+$ and $CD8^+$ to identify T cell subsets in CT2A-luc tumor sections post-treatment (Scale bar: 50 μm). (J) Photographs and (K) weight of the spleens along with (L) body weight of mice from orthotopic CT2A-luc model following various treatments. The data are presented as mean ± SD (n = 3).

recurrence by promoting immunotherapy responses (Figs. 6B, 6C). The strong recurrences of GBM in mice treated with Exo alone or PBS resulted in significant weight loss due to the rapid proliferation of highly aggressive postoperative tumors. In contrast, mice treated with Exo-CpG plus aPD-L1 exhibited an increase in body weight (Figure S19), supporting its good immunosuppressive therapeutic effects without inducing recurrence. In parallel, Exo-CpG combined with aPD-L1 significantly prolonged the survival time of mice, surpassing that of Exo-CpG (39 days), Exo alone (24 days) and PBS (23 days), respectively. Interestingly, Exo-CpG+aPD-L1 treatment resulted in a complete

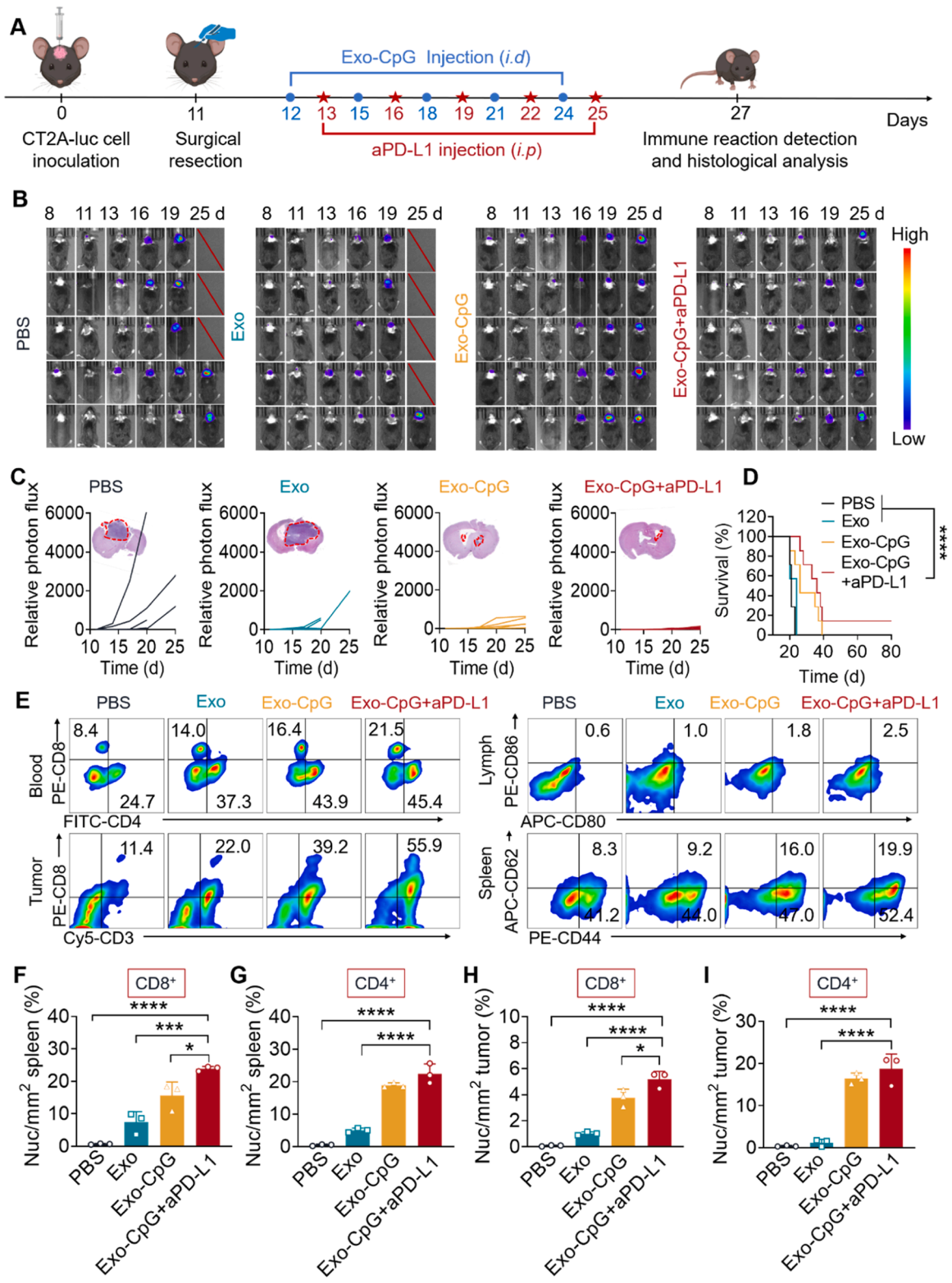

Fig. 6. Therapeutic effect of Exo-CpG in orthotopic CT2A-luc recurrent mouse model. (A) The recurrent tumor model is established by intracranially inoculating CT2A-luc cells, and the tumor is surgically excision on day 11. The treatment groups and dosing regimens were consistent with those outlined for the tumor models described above. (B) Bioluminescence images and (C) relative bioluminescence intensity of the treated mice. (D) Survival curves of the treated mice. (E) Representative flow cytometry dot plots showing $CD4^+$ and $CD8^+$ T cells in the blood (upper left), $CD8^+$ T cells in the tumor (bottom left), CD86 and CD80 in mature DCs (upper right), $CD62^{Low}$ and $CD44^{Hi}$ effector memory T cells in the spleen (bottom right) on day 27. Quantitation of IHC analysis of (F) $CD8^+$ and (G) $CD4^+$ T cells in the spleen tissues. IHC quantitation analysis of (H) $CD8^+$ and (I) $CD4^+$ T cells in the tumor sections on day 27.

recovery of 1 out of 7 mice during the treatment, with survival extending beyond 80 days (Fig. 6D). Similar to the GL261-luc and CT2A-luc models, the combination of Exo-CpG and aPD-L1 induced substantial tumor apoptosis, as evidenced by TUNEL staining (Figure S20). This effectively inhibited tumor recurrence while showing no significant damage to major organs or signs of inflammatory injury (Figure S21). Collectively, Exo-CpG together with aPD-L1 produce potent antitumor effects in the immunosuppressive orthotopic GBM tumor resection model.

Next, we studied the immunostimulatory effect of Exo-CpG in the CT2A-luc-based recurrence model. Flow cytometry results showed that Exo-CpG+aPD-L1 increased the levels of $CD4^+$ and $CD8^+$ T cells in the blood by 2.02-fold and 4.90-fold in the tumor compared with PBS control, respectively (Fig. 6E). We further observed an approximately 4.17-fold increase in mature DCs and a 1.46-fold upsurge in memory T cells following treatment with Exo-CpG+aPD-L1 (Fig. 6E). These results were further corroborated by IHC images of tumor slices and spleen sections (Fig. 6F-6I and Figure S22). Finally, the efficient tumor inhibition induced by Exo-CpG plus aPD-L1 was attributed to the intratumoral activation and alleviation of immunosuppression.

Next, the routine blood and biochemical tests were conducted to assess the long-term biosafety of exosomes. The results showed that the Exo-CpG did not change blood parameters (Figure S23), evidencing the excellent biocompatibility of Exo-CpG.

Conclusion

To sum up, we have successfully developed a versatile and resilient exosomal platform derived from natural GBM tumor cells for the immunotherapy of homologous GBM. These exosomes effectively traverse the BBB via multiple pathways (caveolin-, clathrin-, and micropinocytosis-mediated transcytosis), specifically targeting GBM lesions and infiltrating tumor tissues deeply. With adjuvant CpG modification, Exo-CpG effectively induces cytotoxic T cells ($CD4^+$ and $CD8^+$), and mature dendritic cells ($CD62^{Low}$ and $CD44^{Hi}$) *in vivo*, following *i.d.* injection. Additionally, Exo-CpG elicits strong and long-lasting immune responses due to the presence of various natural homotypic tumor-associated antigens on its surface, promoting the maturation of DCs and facilitating antigen presentation. Notably, Exo-CpG in combination with aPD-L1 yield significant tumor suppression in both orthotopic GL261-luc and immunosuppressive CT2A-luc GBM murine models. More importantly, in the aggressive recurrent GBM model, our exosomal nanoplatform sustains robust immunity, effectively inhibiting GBM tumor cell proliferation, which leads to extending mouse survival up to day 80. Overall, our engineered exosomes offer a simple and powerful strategy for the immunotherapy of GBM.

CRediT authorship contribution statement

Ismail Muhammad: Writing – review & editing, Visualization, Validation. **He Wenya:** Visualization, Validation, Methodology. **Zheng Meng:** Writing – review & editing, Supervision, Conceptualization. **Zou Yan:** Writing – review & editing, Supervision, Project administration, Funding acquisition, Conceptualization. **Shi Bingyang:** Writing – review & editing, Supervision, Funding acquisition, Conceptualization. **Li Shanshan:** Writing – original draft, Methodology, Investigation, Data curation. **Zhang Dongya:** Software, Methodology, Investigation, Funding acquisition. **Wang Yibin:** Validation, Software, Methodology, Investigation.

Author contributions

YZ and **BS** conceived and designed the project. SL performed the experiments and analyzed data. **DZ** and **YW** assisted with the construction of the glioblastoma recurrences mouse model. **SL** and **YZ** prepared the first version of the manuscript. **BS, WH, MI** and **MZ** commented on the manuscript and contributed to the final version.

Declaration of Competing Interest

The authors declare that they have no known competing financial interests or personal relationships that could have appeared to influence the work reported in this paper.

Acknowledgements

This work was supported by National Natural Science Foundation of China (NSFC 32271463, 52073079 and 32101152). Sponsored by Natural Science Foundation of Henan (242300421089), Henan Province Science and Technology Research and Development Program Joint Fund (Advantage Discipline Cultivation) Project (232301420064), the General Financial Grant from the China Postdoctoral Science Foundation (2023M741015) and the Postdoctoral Fellowship Program of CPSF (GZC20230691) and the Henan University Double First-Class Foundation. The schemes were created in the Biorender.com. All animal handling protocols and experiments were approved by the Medical and Scientific Research Ethics Committee of Henan University School of Medicine (P. R. China) (HUSOM-2018-355).

Appendix A. Supporting information

Supplementary data associated with this article can be found in the online version at doi:10.1016/j.nantod.2025.102748.

Data availability

Data will be made available on request.

References

[1] A.T. Yeo, S. Rawal, B. Delcuze, A. Christofides, A. Atayde, L. Strauss, L. Balaj, V. A. Rogers, E.J. Uhlmann, H. Varma, B.S. Carter, V.A. Boussiotis, A. Charest, Single-cell RNA sequencing reveals evolution of immune landscape during glioblastoma progression, Nat. Immunol. 23 (6) (2022) 971–984.
[2] P. Chan, J.N. Rich, S.A. Kay, Watching the clock in glioblastoma, Neuro Oncol. 25 (11) (2023) 1932–1946.
[3] Y. Zou, Y. Liu, Z. Yang, D. Zhang, Y. Lu, M. Zheng, X. Xue, J. Geng, R. Chung, B. Shi, Effective and targeted human orthotopic glioblastoma xenograft therapy via a multifunctional biomimetic nanomedicine, Adv. Mater. 30 (51) (2018) e1803717.
[4] Q.-X. Huang, J.-L. Liang, M.-T. Niu, X.-K. Jin, C.-Y. Dong, S.-X. Cheng, X.-Z. Zhang, Interfering tumor metabolism by bimetallic nanoagent for amplifying nanocatalytic-mediated glioblastoma immunotherapy, Nano Today 56 (2024).
[5] X. Li, Y. Lan, X. Fu, X. Luo, J. Chen, W. Zhang, B. Zuo, T. Yang, B. Liu, C. Zhang, H. Guo, DNA nanomachine-driven chemodynamic therapy against glioblastoma, Aggregate (2024), https://doi.org/10.1002/agt2.603.
[6] C. Zhang, J. Song, L. Lou, X. Qi, L. Zhao, B. Fan, G. Sun, Z. Lv, Z. Fan, B. Jiao, J. Yang, Doxorubicin-loaded nanoparticle coated with endothelial cells-derived exosomes for immunogenic chemotherapy of glioblastoma, Bioeng. Transl. Med. 6 (3) (2021) e10203.
[7] A.M. Knudsen, B. Halle, O. Cedile, M. Burton, C. Baun, H. Thisgaard, A. Anand, C. Hubert, M. Thomassen, S.R. Michaelsen, B.B. Olsen, R.H. Dahlrot, R. Bjerkvig, J. D. Lathia, B.W. Kristensen, Surgical resection of glioblastomas induces pleiotrophin-mediated self-renewal of glioblastoma stem cells in recurrent tumors, Neuro Oncol. 24 (7) (2022) 1074–1087.
[8] D.A. Reardon, A.A. Brandes, A. Omuro, P. Mulholland, M. Lim, A. Wick, J. Baehring, M.S. Ahluwalia, P. Roth, O. Bähr, S. Phuphanich, J.M. Sepulveda, P. De Souza, S. Sahebjam, M. Carleton, K. Tatsuoka, C. Taitt, R. Zwirtes, J. Sampson, M. Weller, Effect of nivolumab vs bevacizumab in patients with recurrent glioblastoma, JAMA Oncol. 6 (7) (2020) 1003–1010.
[9] X. Wang, G. Guo, H. Guan, Y. Yu, J. Lu, J. Yu, Challenges and potential of PD-1/PD-L1 checkpoint blockade immunotherapy for glioblastoma, J. Exp. Clin. Cancer Res. 38 (2019) 87.
[10] H. Li, J. Zhang, M. Tan, Y. Yin, Y. Song, Y. Zhao, L. Yan, N. Li, X. Zhang, J. Bai, T. Jiang, H. Li, Exosomes based strategies for cardiovascular diseases: opportunities and challenges, Biomaterials 308 (2024) 122544.
[11] Y. Ai, C. Guo, M. Garcia-Contreras, L.S. Sánchez B, A. Saftics, O. Shodubi, S. Raghunandan, J. Xu, S.J. Tsai, Y. Dong, R. Li, T. Jovanovic-Talisman, S.J. Gould, Endocytosis blocks the vesicular secretion of exosome marker proteins, Sci. Adv. 10 (19) (2024) eadi9156.
[12] I. Cela, E. Capone, G. Trevisi, G. Sala, Extracellular vesicles in glioblastoma: biomarkers and therapeutic tools, Semin. Cancer Biol. 101 (2024) 25–43.

[13] X. Hao, S. Wang, L. Wang, J. Li, Y. Li, J. Liu, Exosomes as drug delivery systems in glioma immunotherapy, J. Nanobiotechnol. 22 (1) (2024) 340.
[14] M. Shao, D. Lopes, J. Lopes, S. Yousefiasl, A. Macário-Soares, D. Peixoto, I. Ferreira-Faria, F. Veiga, J. Conde, Y. Huang, X. Chen, A.C. Paiva-Santos, P. Makvandi, Exosome membrane-coated nanosystems: exploring biomedical applications in cancer diagnosis and therapy, Matter 6 (3) (2023) 761–799.
[15] N. Perets, O. Betzer, R. Shapira, S. Brenstein, A. Angel, T. Sadan, U. Ashery, R. Popovtzer, D. Offen, Golden exosomes selectively target brain pathologies in neurodegenerative and neurodevelopmental disorders, Nano Lett. 19 (6) (2019) 3422–3431.
[16] Z. Xu, S. Zeng, Z. Gong, Y. Yan, Exosome-based immunotherapy: a promising approach for cancer treatment, Mol. Cancer 19 (1) (2020) 160.
[17] R. Wang, Q. Liang, X. Zhang, Z. Di, X. Wang, L. Di, Tumor-derived exosomes reversing TMZ resistance by synergistic drug delivery for glioma-targeting treatment, Colloids Surf. B Biointerfaces 215 (2022) 112505.
[18] L. Qiao, S. Hu, K. Huang, T. Su, Z. Li, A. Vandergriff, J. Cores, P.-U. Dinh, T. Allen, D. Shen, H. Liang, Y. Li, K. Cheng, Tumor cell-derived exosomes home to their cells of origin and can be used as trojan horses to deliver cancer drugs, Theranostics 10 (8) (2020) 3474–3487.
[19] Y. Wang, Q. Ma, T. Wang, J. Xing, Q. Li, D. Wang, G. Wang, The involvement and application potential of exosomes in breast cancer immunotherapy, Front. Immunol. 15 (2024) 1384946.
[20] M. Morishita, Y. Takahashi, A. Matsumoto, M. Nishikawa, Y. Takakura, Exosome-based tumor antigens-adjuvant co-delivery utilizing genetically engineered tumor cell-derived exosomes with immunostimulatory CpG DNA, Biomaterials 111 (2016) 55–65.
[21] M. Yang, J. Zhou, L. Lu, D. Deng, J. Huang, Z. Tang, X. Shi, P.C. Lo, J.F. Lovell, Y. Zheng, H. Jin, Tumor cell membrane-based vaccines: a potential boost for cancer immunotherapy, Exploration 4 (6) (2024) 20230171.
[22] F.U. Rehman, Y. Liu, Q. Yang, H. Yang, R. Liu, D. Zhang, P. Muhammad, Y. Liu, S. Hanif, M. Ismail, M. Zheng, B. Shi, Heme Oxygenase-1 targeting exosomes for temozolomide resistant glioblastoma synergistic therapy, J. Control. Release 345 (2022) 696–708.
[23] Z. Wang, H. Qing, R. Li, X. Li, X. Guo, S. Zhou, M2 Macrophage-derived exosomes inhibiting neutrophil extracellular traps for ischemic stroke therapy, Adv. Funct. Mater. 34 (42) (2024) 2402724.
[24] T. Wu, Y. Liu, Y. Cao, Z. Liu, Engineering macrophage exosome disguised biodegradable nanoplatform for enhanced sonodynamic therapy of glioblastoma, Adv. Mater. 34 (15) (2022) 2110364.
[25] P. Bao, H.-Y. Gu, Y.-C. Jiang, J.-W. Wang, M. Wu, A. Yu, Z. Zhong, X.-Z. Zhang, In situ sprayed exosome-cross-linked gel as artificial lymph nodes for postoperative glioblastoma immunotherapy, ACS Nano 18 (20) (2024) 13266–13276.
[26] P. Bao, H.Y. Gu, J.J. Ye, J.L. He, Z. Zhong, A.X. Yu, X.Z. Zhang, Chimeric exosomes functionalized with STING activation for personalized glioblastoma immunotherapy, Adv. Sci. 11 (6) (2023) 2306336.
[27] F.U. Rehman, Y. Liu, M. Zheng, B. Shi, Exosomes based strategies for brain drug delivery, Biomaterials 293 (2023) 121949.
[28] Y. Yan, X. Huang, L. Yuan, T. Ngai, G. Ma, Y. Xia, Dictating the spatial-temporal delivery of molecular adjuvant and antigen for the enhanced vaccination, Biomaterials 311 (2024) 122697.
[29] X. Xue, H. Qu, Y. Li, Stimuli-responsive crosslinked nanomedicine for cancer treatment, Exploration 2 (6) (2022) 20210134.
[30] X. Zhi, P. Yang, Y. Xu, Z. Dai, X. Yue, L. Qian, Toll-like receptor-targeted nanoparticles: a powerful combination for tumor immunotherapy, Nano Today 53 (2023) 102003.
[31] J. Wang, P. Chen, Y. Dong, H. Xie, Y. Wang, F. Soto, P. Ma, X. Feng, W. Du, B.F. Liu, Designer exosomes enabling tumor targeted efficient chemo/gene/photothermal therapy, Biomaterials 276 (2021) 121056.
[32] Q. Lv, L. Cheng, Y. Lu, X. Zhang, Y. Wang, J. Deng, J. Zhou, B. Liu, J. Liu, Thermosensitive exosome-liposome hybrid nanoparticle-mediated chemoimmunotherapy for improved treatment of metastatic peritoneal cancer, Adv. Sci. 7 (18) (2020) 2000515.
[33] T. Lyu, Y. Wang, D. Li, H. Yang, B. Qin, W. Zhang, Z. Li, C. Cheng, B. Zhang, R. Guo, Y. Song, Exosomes from BM-MSCs promote acute myeloid leukemia cell proliferation, invasion and chemoresistance via upregulation of S100A4, Exp. Hematol. Oncol. 10 (1) (2021) 24.
[34] C. Gong, X. Zhang, M. Shi, F. Li, S. Wang, Y. Wang, Y. Wang, W. Wei, G. Ma, Tumor exosomes reprogrammed by low pH are efficient targeting vehicles for smart drug delivery and personalized therapy against their homologous tumor, Adv. Sci. 8 (10) (2021) 2002787.
[35] A. Thakur, D.C. Parra, P. Motallebnejad, M. Brocchi, H.J. Chen, Exosomes: small vesicles with big roles in cancer, vaccine development, and therapeutics, Bioact. Mater. 10 (2022) 281–294.
[36] R. Isaac, F.C.G. Reis, W. Ying, J.M. Olefsky, Exosomes as mediators of intercellular crosstalk in metabolism, Cell Metab. 33 (9) (2021) 1744–1762.
[37] G. Catania, G. Rodella, K. Vanvarenberg, V. Préat, A. Malfanti, Combination of hyaluronic acid conjugates with immunogenic cell death inducer and CpG for glioblastoma local chemo-immunotherapy elicits an immune response and induces long-term survival, Biomaterials 294 (2023) 122006.
[38] F. Li, X. Ding, Z. Lv, J. Li, D. Yang, A DNA-polymer hybrid nanocomplex based bi-adjuvant vaccine for tumor immunotherapy, Nano Today 54 (2024) 102061.
[39] S.F. Liang, F.F. Zuo, B.C. Yin, B.C. Ye, Delivery of siRNA based on engineered exosomes for glioblastoma therapy by targeting STAT3, Biomater. Sci. 10 (6) (2022) 1582–1590.
[40] S. Shan, J. Chen, Y. Sun, Y. Wang, B. Xia, H. Tan, C. Pan, G. Gu, J. Zhong, G. Qing, Y. Zhang, J. Wang, Y. Wang, Y. Wang, P. Zuo, C. Xu, F. Li, W. Guo, L. Xu, M. Chen, Y. Fan, L. Zhang, X.J. Liang, Functionalized macrophage exosomes with panobinostat and PPM1D-siRNA for diffuse intrinsic pontine gliomas therapy, Adv. Sci. 9 (21) (2022) e2200353.
[41] Y. Liang, Z. Iqbal, J. Lu, J. Wang, H. Zhang, X. Chen, L. Duan, J. Xia, Cell-derived nanovesicle-mediated drug delivery to the brain: principles and strategies for vesicle engineering, Mol. Ther. 31 (5) (2022) 1207–1224.
[42] Y. Wang, Y. Huo, C. Zhao, H. Liu, Y. Shao, C. Zhu, L. An, X. Chen, Z. Chen, Engineered exosomes with enhanced stability and delivery efficiency for glioblastoma therapy, J. Control. Release 368 (2024) 170–183.
[43] Y. Zhuo, Z. Luo, Z. Zhu, J. Wang, X. Li, Z. Zhang, C. Guo, B. Wang, D. Nie, Y. Gan, G. Hu, M. Yu, Direct cytosolic delivery of siRNA via cell membrane fusion using cholesterol-enriched exosomes, Nat. Nanotechnol. 19 (12) (2024) 1858–1868.
[44] I. Kimiz-Gebologlu, S.S. Oncel, Exosomes: large-scale production, isolation, drug loading efficiency, and biodistribution and uptake, J. Control. Release 347 (2022) 533–543.
[45] Z. Dai, Q. Wang, J. Tang, M. Wu, H. Li, Y. Yang, X. Zhen, C. Yu, Immune-regulating bimetallic metal-organic framework nanoparticles designed for cancer immunotherapy, Biomaterials 280 (2022) 121261.
[46] L. Guo, H. Chen, J. Ding, P. Rong, M. Sun, W. Zhou, Surface engineering salmonella with pH-responsive polyserotonin and self-activated DNAzyme for better microbial therapy of tumor, Exploration 3 (6) (2023) 20230017.
[47] B. Chen, K. Guo, X. Zhao, Z. Liu, C. Xu, N. Zhao, F.J. Xu, Tumor microenvironment-responsive delivery nanosystems reverse immunosuppression for enhanced CO gas/immunotherapy, Exploration 3 (6) (2023) 20220140.
[48] J. Yang, X. Pan, J. Zhang, S. Ma, J. Zhou, Z. Jia, Y. Wei, Z. Liu, N. Yang, Q. Shen, Reprogramming dysfunctional dendritic cells by a versatile metabolism nano-intervenor for enhancing cancer combinatorial immunotherapy, Nano Today 46 (2022) 101618.
[49] J. Wei, D. Wu, S. Zhao, Y. Shao, Y. Xia, D. Ni, X. Qiu, J. Zhang, J. Chen, F. Meng, Z. Zhong, Immunotherapy of malignant glioma by noninvasive administration of TLR9 agonist CpG nano-immunoadjuvant, Adv. Sci. 9 (13) (2022) e2103689.
[50] G. Cui, Y. Sun, L. Qu, C. Shen, Y. Sun, F. Meng, Y. Zheng, Z. Zhong, Uplifting antitumor immunotherapy with lymph-node-targeted and ratio-controlled codelivery of tumor cell lysate and adjuvant, Adv. Healthc. Mater. 13 (17) (2024) 2303690.
[51] H. Kinoh, S. Quader, H. Shibasaki, X. Liu, A. Maity, T. Yamasoba, H. Cabral, K. Kataoka, Translational nanomedicine boosts anti-PD1 therapy to eradicate orthotopic PTEN-negative glioblastoma, ACS Nano 14 (8) (2020) 10127–10140.
[52] T. Shan, W. Wang, M. Fan, J. Bi, T. He, Y. Sun, M. Zheng, D. Yan, Effective glioblastoma immune sonodynamic treatment mediated by macrophage cell membrane cloaked biomimetic nanomedicines, J. Control. Release 370 (2024) 866–878.
[53] W. Wu, J.L. Klockow, M. Zhang, F. Lafortune, E. Chang, L. Jin, Y. Wu, H. E. Daldrup-Link, Glioblastoma multiforme (GBM): an overview of current therapies and mechanisms of resistance, Pharmacol. Res. 171 (2021) 105780.